Journal of Physics: Conference Series **500** (2014) 192023 doi:10.1088/1742-6596/500/19/192023

# Two-temperature hydrodynamic expansion and coupling of strong elastic shock with supersonic melting front produced by ultrashort laser pulse

**Nail A Inogamov**[1], **Vasily V Zhakhovsky**[2,3], **Viktor A Khokhlov**[1], **Brian J Demaske**[3], **Konstantin V Khishchenko**[2] **and Ivan I Oleynik**[3]

[1] Landau Institute for Theoretical Physics, Russian Academy of Sciences, Russian Federation
[2] Joint Institute for High Temperatures of Russian Academy of Sciences, Russian Federation
[3] Department of Physics, University of South Florida, Tampa, Florida, USA

E-mail: nailinogamov@gmail.com

**Abstract.** Ultrafast processes, including nonmonotonic expansion of material into vacuum, supersonic melting and generation of super-elastic shock wave, in a surface layer of metal irradiated by an ultrashort laser pulse are discussed. In addition to the well-established two-temperature (2T) evolution of heated layer a new effect of electron pressure gradient on early stage of material expansion is studied. It is shown that the expanding material experiences an unexpected jump in flow velocity in a place where stress exceeds the effective tensile strength provided by used EoS of material. Another 2T effect is that supersonic propagation of homogeneous melting front results in distortion of spatial profile of ion temperature, which later imprints on ion pressure profile transforming in a super-elastic shock wave with time.

## 1. Introduction

Ultrafast (supersonic) heating of thin surface layer during a two-temperature state increases pressure in this layer simultaneously with the rise of energy density (see [1], Fig. 8 in this paper and references therein). In a range of absorbed energies $F_{abs} \sim 30 - 200$ mJ/cm$^2$, typical for technological applications, the energy density in a heated layer is $\sim 10^{10}$ J m$^{-3}$ $= 10$ GPa. Corresponding pressures are of the order of pressures behind detonation waves in high explosives. Thus, an ultrashort laser pulse (usLP) transfers a thin surface layer to a state similar to one in explosion. This is a key point for shock-wave generation, micromachining, laser pinning, usLP microsurgery, art cleaning etc. A fundamental understanding of usLP action is necessary to optimize all such technologies. Two problems are considered in this short report: (i) an early stage of expansion under action of electronic pressure $p_e$, and (ii) a thermomechanical coupling which combines homogeneous melting and generation of compression wave. Late time evolution, including elastic-plastic transformations in an evolving compression wave, focusing of characteristics and shock-wave formation, is beyond the scope of this research.

## 2. Rarefaction at two-temperature stage

It is well known that usLP transfers metal into two-temperature (2T) state, see [1] and references therein. Electron temperature $T_e(x,t)$ increases during usLP. After the end of usLP, the

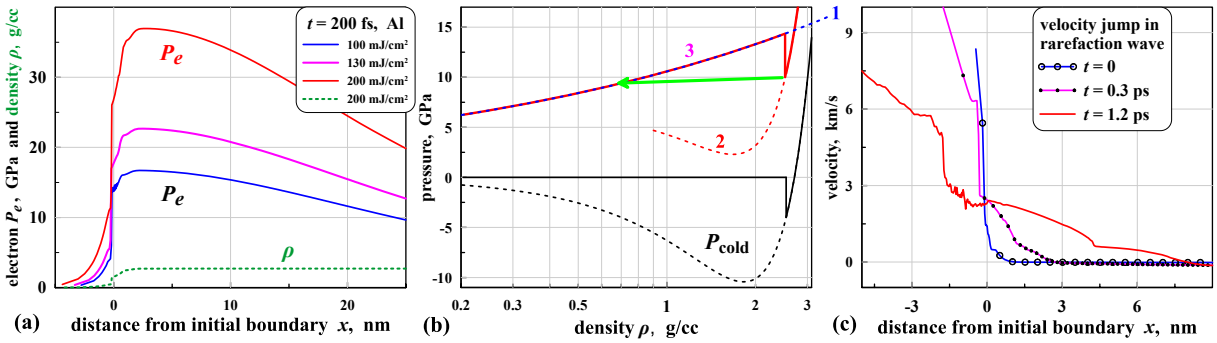


**Figure 1.** (a) Profiles of electron pressures $p_e(x, t = 200\,\text{fs})$ in aluminum for $F_{abs} = 100, 130,$ and 200 mJ cm$^{-2}$. The corresponding ratios $(p_e)_{max}/(p_i)_{max}$ are 3.5, 3.7, and 4.3. Electron pressures exceed the maximum tensile strength $\approx$ 11 GPa of Al. The green line is density profile $\rho(x, t = 200\,\text{fs})$. There is a rarefaction jump (RFJ) sharply decreasing density in the point $x = -0.2$ nm. The RFJ corresponds to the place where pressure drops steeply. (b) Black lines show cold curves $p_i(\rho, T_i = 0)$. At densities below the density $\rho_{sp}$ the cold pressure is equal to zero. Pressure $p_e$ marked by the "1" slowly decreases $\propto \rho^{1/3}$ when $\rho$ decreases. Solid red line 3 shows a total pressure. Dashed curve 2 is a total pressure extended beyond the effective tensile strength. Sharp jump of ion pressure, when it reaches the effective strength at $\rho_{sp}$, leads to the RFJ. This causes formation of a pronounced bump in the total pressure $p = p_e + p_i$ as a function of density. RFJ results in rarefaction shock (shown as a green arrow), which virtually transfers material under "pressure barrier". (c) Shape of RFJ on velocity profiles from 2T-HD modeling. Velocities of inflow into RFJ are $\approx$ 1.5 km/s. Jump of velocity is approximately the same value. Markers at profiles present a chain of Lagrangian nodes used in our 2T-HD code.

temperature $T_e$ near surface begin to decrease due to energy transfer to ion subsystem and due to electron heat conduction into bulk. While ion temperature $T_i(x, t)$ gradually increases during electron-ion relaxation process. Let us consider rarefaction into vacuum during the 2T stage, when motion of material is driven mainly by electron pressure $p_e$. Usually peoples pay small attention to this effect saying that it is short in time and that mass ablated during this stage is small in comparison with mass ablated at one-temperature (1T) stage. Reasons to consider this effect here are: (i) The effect noticeable at high electron temperatures $T_e$ and hence high electron pressures; (ii) It seems that atoms of metal tear off from bulk metal in excited electronic state - before they decrease their temperature $T_e \sim$ few eV through electron-ion collisional coupling inside dense metal. Perhaps, this is an example where small but macroscopic amount of matter (stretched up to gaseous state) appears as excited atoms. In the range of ion temperatures from 0.3 kK to few kK, which established at the end of a 2T stage, metals evaporate during 1T stage from a surface as neutrals in low density vapor; and (iii) It is interesting to consider hydrodynamic motion of 2T material.

Profiles of electron pressure at times slightly after the maximums of their values at the end of an absorption stage are shown in figure 1(a), where pulse duration is $\tau_L = 100$ fs. Laser pulse has a Gaussian shape, and it is absorbed in a skin layer with depth $\delta$. Corresponding energy source is $\dot{E}_L = F_{abs}/(\sqrt{\pi}\tau_L\delta)\exp(-t^2/\tau_L^2)\exp(-x/\delta)\theta(x)$ W m$^{-3}$, $\theta(x) = 1$ if $x > 0$ and 0 if $x < 0$. Maximum electron pressure $p_e$ grows approximately proportionally to the absorbed energy $F_{abs}$, see figure 1(a). We see that values of $p_e$ are high, comparable with bulk modulus $K$, while ion pressures $p_i$ are significantly less in the 2T stage. Corresponding instant maximum temperatures $(T_e, T_i)$ in kK are (24.4, 1.2), (29, 1.3), and (38, 1.46) for profiles shown in figure 1(a). The main feature of figure 1(a) is a sharp density decrease (rarefaction jump - RFJ) in a very narrow area, almost in a point. What is more, the ratio of densities at the right and left

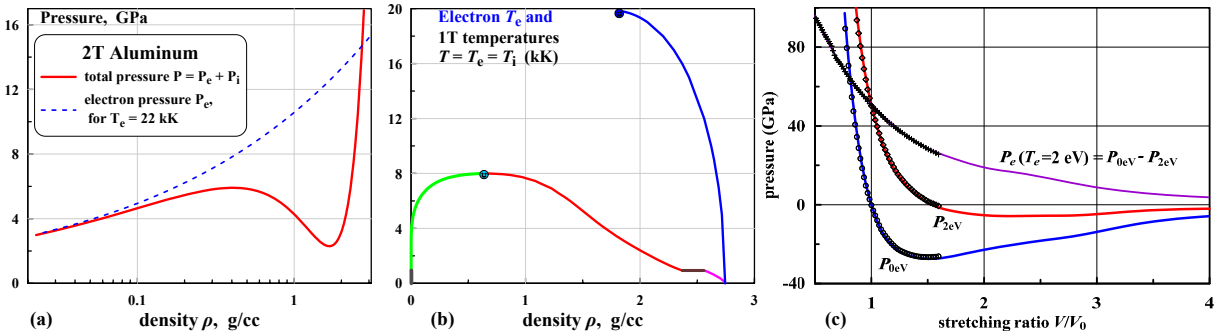


**Figure 2.** (a) Total pressure in Al system where voids are not allowed to nucleate because the background electron pressure is always positive. Thus, $p_e$ preserves condense phase from transition to two-phase mixture, and a smooth pressure well appears. It is not obvious how such 2T system will proceed further when it expands up to the minimum of this well. Results of DFT and MD simulations are presented below to address this issue. Ion contribution to the total pressure is calculated for low ion temperature (cold curve). (b) Phase diagram of 2T EOS of Al. Unlike 1T EOS depending on two variables the 2T EOS depends on three variables $(\rho, T_e, T_i)$. Therefore, 2T phase diagram is 3D diagram. Two projections of this 3D diagram are shown: 1T plane with equal temperatures $T = T_i = T_e$, and plane with cold ion subsystem $T_i = 0$. (c) Total and electron pressures in nickel with cold ions: $p(V)$ for $T_e = 0$ and 2 eV, and $p_e(V)$ for $T_e = 2$ eV; $V = 1/\rho$, see details in text.

sides of the RFJ is finite, metal at the left side is still dense $\approx 0.6$ g cm$^{-3}$.

The RFJ shown in figure 1 is produced by a sharp drop of resistance of material against stretching, when metal is expanded by electron pressure $p_e$ beyond the density $\rho_{sp}$ corresponding to the effective tensile strength specified in the used EoS. We come to this conclusion about sharp drop and RFJ while using standard three assumptions, see, e.g. [2]. They are (i) $p(\rho, T_e, T_i) = p_e(\rho, T_e) + p_i(\rho, T_i)$; (ii) pressure $p(\rho, T)$ from 1T EoS is taken as a function $p_i(\rho, T_i)$ with $T = T_i$; and (iii) electron pressure calculated from density functional theory (DFT) is taken as a function $p_e(\rho, T_e)$, see [2] and references therein, and our DFT data presented below. Those assumptions are approximately adequate for description of 1T stage outside the neighborhood of ablation threshold, where foam stretch makes notable contribution to expansion dynamics. The 1T stage follows the 2T stage. At the 1T stage an influence of electron pressure $p_e$ becomes insignificant. But at the 2T stage existence of pressure $p_e$ is crucial. This pressure squeezes voids nucleating when density drops below the density $\rho_{sp}$. Thus an electron pressure external to nuclei suppresses nucleation. Therefore it seems that the non-zero continuation of a cold curve above a specific volume $1/\rho_{sp}$ takes place, see figure 2(a).

Phase diagram of 2T EOS is presented in figure 2(b). Projection of 2T EOS on the plane $(\rho, T_e, T_i = 0)$ is calculated from condition of electron and ion pressure balance at the binodal: $-p_i(\rho, T_i = 0) = p_e(\rho, T_e)$, where the cold pressure curve for Al is taken from Rose EoS [3]. The roots of this equation $T_e(\rho)$ define the projection of binodal plotted in figure 2(b), the blue curve. We see how electron pressure growing with increase of $T_e$ blows cold lattice. The end point of the 2T binodal $(T_e)_{cr}$ is shown as a blue circle in figure 2(b). In this point (2T critical point) a lattice loses stability, because electron pressure exceeds lattice cohesion.

There is no dispersal of matter from a boundary below the electron critical point $(T_e)_{cr}$ in case of cold lattice $T_i = 0$. Metal expands up to electronic binodal (blue curve in figure 2(b)) where total pressure equals to zero. This binodal forms a moving boundary of a metal. On the contrary, for temperatures higher than $(T_e)_{cr}$ the flow loses the jump of density at a boundary and expands as gaseous medium, since above this temperature the binodal (separating

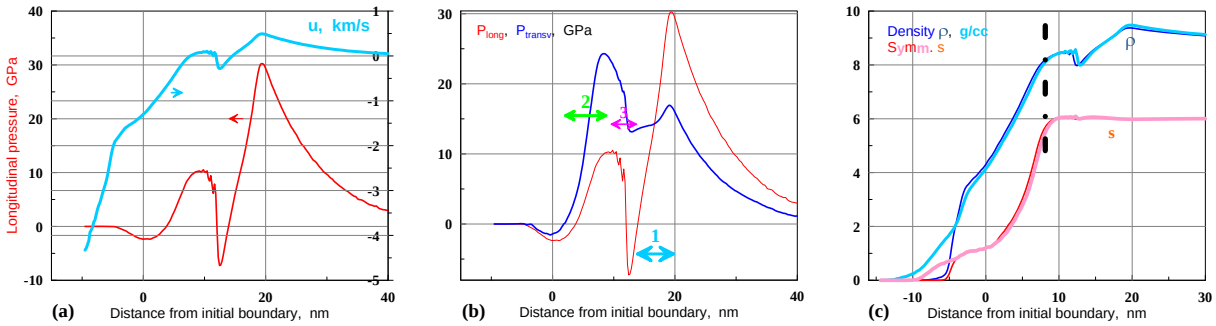


**Figure 3.** MD simulation of expansion of Ni obeying the electron isotherms from DFT calculations shown in figure 2(c). Initial exponential profile $T_e(x, t = 0) = T_0 \exp(-x/\delta)$ with a skin depth $\delta = 14.5$ nm and electron surface temperature $T_0 = 2.5$ eV has been imposed on a freestanding film 60 nm thick. The local values of $T_e$ are conserved in Lagrangian particles. Electron-ion cooling of electrons and electron heat conduction loses are neglected during early stage. Surprising phenomenon of *deceleration* of expansion flow into vacuum is discussed in text. All profiles are at $t = 2.56$ ps. (a) Flow velocity and longitudinal stress. (b) Longitudinal and transverse stress. (c) Profiles of density and centro-symmetry parameter $s$ for two cases: one is below electron critical point with initial electron surface temperature $T_0 = 2.4$ eV and other is above this point, its $T_0 = 3$ eV. Above a critical value a powerful flux of atoms in gas appears, compare density distributions and distributions of parameter $s$ in those two cases. Those atoms transfer into gas in excited states - since their electron temperatures remain finite.

condensed matter and vapor) disappears. DFT and molecular dynamics (MD) simulations have been carried to understand the problem concerning 2T expansion.

A family of dependencies of total pressure $p(\rho, T_e, T_i = 0)$ on density have been obtained from DFT calculations presented in figure 2(c). It was supposed that fcc lattice temperature of nickel is zero ($T_i = 0$); see similar approach developed in [2, 4, 5]. Dependencies of pressure $p(\rho, T_e, T_i = 0)$ on density have been parameterized by temperature $T_e$. Example from this family is shown in figure 2(c). The condition $p_e(\rho, T_e) = p(\rho, T_e, T_i = 0) - p(\rho, T_e = 0, T_i = 0)$ is used to calculate electron pressure [2, 4, 5]. The curves in figure 2(c) correspond to the undercritical case when parameter $T_e$ is below the critical value $(T_e)_{cr}$. Therefore some cohesion remains. It was found that a critical value belong to the interval $2.5\,\text{eV} < (T_e)_{cr} < 3\,\text{eV}$.

Let's present results of MD simulations. They show a surprising picture where even increase of longitudinal stress along direction of expansion takes place! This increase (see figure 3(a)) looks like an increase of pressure in figure 2(a). In figure 2(a) pressure increases to the left side from the minimum. The increase of longitudinal stress in figure 3(a) causes deceleration of expansion flow obvious from velocity profile $u(x, t = 2.56\,\text{ps})$ in figure 3(a). What is the reason of such unusual increase of stress during rarefaction into vacuum?

The reason is connected with uniaxial stretching of single crystal and subsequent elastic relaxation. Qualitatively it is similar to the plastic wave considered in [6, 7]. Longitudinal expansion at stage 1 shown in figure 3(b) creates strong uniaxial stretching of fcc crystal along 110 direction. This stretching decreases longitudinal stress $p_{long}$ at the interval 1 in figure 3(b). While transverse stress $p_{transv}$ decreases more slowly with density drop than longitudinal stress at the interval 1. In case of expansion in direction 110 the components $p_{yy}$ and $p_{zz}$ equal each other. In the bulk metal all three components equal each other. At stage 2 an anisotropic dilution of a crystal cell provokes strong relaxation which releases transverse elastic energy and unloads transverse stresses. This release proceeds through dislocation dynamics and plastic transformations gradually rotating crystal cells and decreasing their uniaxial deformation.

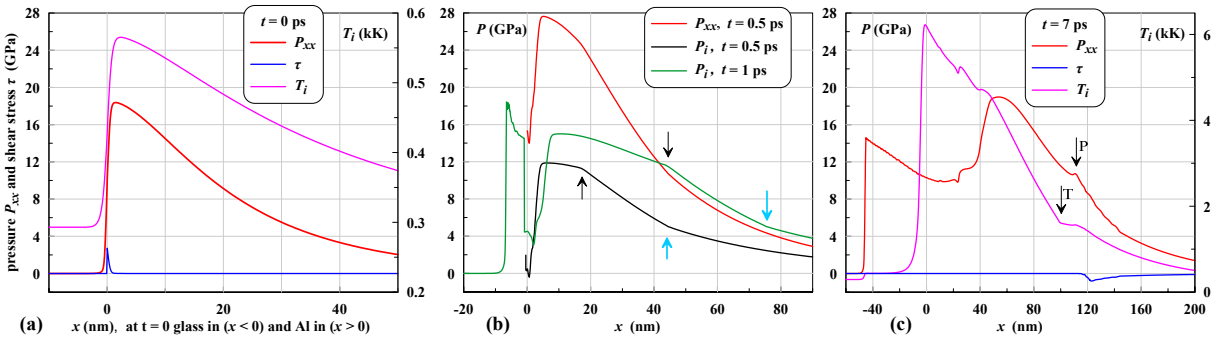


**Figure 4.** (a) Longitudinal stress $p_{xx}$, shear stress $\tau$, and ion temperature $T_i$ at $t = 0$ ps. Time is reckoned from maximum of Gaussian usLP with duration $\tau_L = 100$ fs. Maximum electron temperature for this instant is $T_e = 25$ kK. Temperature before usLP arrival is $T_i = T_e = 0.293$ kK. Motion in this very early times is confined in $\sim 1$ nm thick transition layer between glass and Al. Therefore, stress $\tau$ connected with uniaxial compression is localized in this layer. (b) Profile $p_{xx}$ corresponds to total pressure including ion, electron, and shear stress contributions. Shear stress is negligibly small at the isochoric stage. Shear near glass-Al boundary visible in previous figure disappears as a result of melting. Ion temperature $T_i$ and pressure $p_i$ are tightly coupled at early 2T stage. Average velocity of liquidus marked by black arrows at time interval 0.3-0.5 ps is 78 km/s and at time interval 0.5-1 ps is 55 km/s. The kinks on $T_i$ and $p_i$ profiles are located in the same liquidus and solidus points and moves together at the same velocity. Maximum pressure $p_i$ grows as a result of heat transfer from electron thermal bath, while values $p_i$ in liquidus and solidus are approximately the same. (c) Separation of thermal and acoustic waves, compare the point liquidus "T" at a temperature profile and a trace of liquidus in a point "P" moving along elastic characteristics. Slope of pressure $p$ above a point "P" is twice lower than a slope below this point. Therefore, elastic shock has stress $\approx 12$ GPa when it appears. Solid to the right from a molten zone is in uniaxially compressed state, see non-zero shear stress.

Plastic processes decreases centro-symmetry parameter in the interval 2. The dash-dot line in figure 3(c) marks transition from the interval 2 to the interval 3. We see that centro-symmetry parameter begins to drop steeply in the interval 2. The relaxation of transverse stress takes place mainly at the interval 2. Solid state corresponds to $1 < s \leq 6$, liquid is located in the range $0 < s < 1$, and there is $s = 0$ in gas . Energy release increases longitudinal stress $p_{long}$ in the interval 2 in figure 3(b). The increase of $p_{long}$ inside the interval 2 creates a wave 3 propagating against expansion flow. The wave 3 acts as a decelerator of expansion into vacuum in the interval 3 significantly ahead relative to the production interval 2. Let us emphasize that structure with plastic decay of uniaxially stretched crystal and release of transverse elastic energy is clearly seen beginning from as early instant as 250 fs.

## 3. Imprint of supersonic melting into irradiated nonlinear acoustic wave

The thermodynamic connection (Gruneisen parameter) between internal energy and pressure in isochorically heated matter is different for solid, two-phase solid-liquid, and liquid phases [8, 9]. Therefore, a smooth energy profile, produced by electron conduction and electron-ion (e-i) transfer in isochoric conditions, generates a profile of ion pressure $p_i$ which is peculiar in a two-phase solid-liquid layer. This is a reason for deformation of profile in a two-phase layer where a more steep piece of profile forms. At the end of 2T stage, the ion pressure becomes dominant in a sum $p = p_e + p_i$. Gradient of total pressure $p$ moves matter. Therefore above a melting threshold the pressure profiles $p(x, t)$ have this deformation connected with homogeneous melting. As was said, the deformation is a piece of profile with more steep pressure gradient $p_x$. This piece

propagates into bulk along characteristics and provokes early overturning of elastic part of compression wave into strong elastic shock. This means that dependence of duration of temporal interval needed for overturning on fluence has a jump at a melting threshold, since a profile $p_i$ below melting is smooth (a steep piece disappears) and an overturning happens significantly later.

Imprint of fast melting into generated compression wave has been considered in [8, 9]. But those works were based on hydrodynamic code with *plastic* 2T EOS - role of the imprint for formation of *elastic* shock remains unaddressed. Transition from homogeneous melting to heterogeneous melting and separation of elastic-plastic compression wave during this transition have been considered in great detail in reference [1]. Here we perform hydrodynamic analysis of a 2T stage combined with elasticity effects. It allows in a continuous manner link an early 2T hydrodynamics (2t-HD) with a later development in a partially plastic (molten), partially elastic (solid crystal) media. Figure 4 shows a sequence of processes initiated by usLP $\tau_L = 100$ fs, $F_{abs} = 130$ mJ cm$^{-2}$ transmitted through thick (150 um) glass window and absorbed near glass-Al boundary in aluminum. Model of isotropic elastic medium is added to a 2T plastic EOS for description of motion in crystal. We neglect heat conduction and elasticity in glass.

Hypersonic character of melting front at an early 2T stage is illustrated in figure 4(b). Here we call liquidus as a melting front since it bounds pure melt. Of course this is phase or apparent velocity connected with homogeneous melting under action of heat flux injected into ionic subsystem from hot electrons through electron-ion (e-i) energy transfer. While electron thermal transport is governed by electrons moving with Fermi velocity $\sqrt{2E_F/m_e} \approx 2000$ km/s in Al. Melting zone where crystal gradually melts into liquid is wide - this is a layer between black (liquidus) and blue (solidus) arrows in figure 4(b). It is filled with crystal-melt mixture. Relative partial volume of liquid in mixture gradually increases to 100%. Pure liquid is to the left of the black arrow. In MD simulation the positions of liquidus are approximately the same, while the kink at the solidus is smeared. Figure 4(c) demonstrates how liquidus and its acoustic image gradually separate in space. Visible separation begins at $t \approx 5$ ps, significantly later than the end of electron-ion temperature equilibration.

## Acknowledgments

Support from RFBR is acknowledged (N. A. I., V. A. Kh. grant 13-02-01078; K. V. Kh. grants 11-08-01225, 13-02-91057, 13-08-12248). V. V. Z and I. I. O. were supported by the NSF through grant No. DMR-1008676.

## References

[1] Demaske B J, Zhakhovsky V V, Inogamov N A and Oleynik I I 2013 *Phys. Rev.* B **87** 054109 1–9
[2] Inogamov N A et al. 2012 *AIP Conf. Proc.* **1464** 593–608
[3] Rose J H, Smith J R, Guinea F and Ferrante J 1984 *Phys. Rev.* B **29** 2963
[4] Khakshouri S, Alfe D and Duffy D M 2008 *Phys. Rev.* B **78** 224304
[5] Sin'ko G V, Smirnov N A, Ovechkin A A, Levashov P R and Khishchenko K V 2013 *High Energy Density Physics* **9** 309–314
[6] Anisimov S I, Zhakhovskii V V, Inogamov N A, Nishihara K, Oparin A M and Petrov Y V 2003 *JETP Lett.* **77** 606–610
[7] Anisimov S I, Zhakhovskii V V, Inogamov N A, Nishihara K and Petrov Y V 2007 *Appl. Surf. Sci.* **253** 6390–6393
[8] Inogamov N A, Ashitkov S I, Zhakhovsky V V, Shepelev V V, Khokhlov V A, Komarov P S, Agranat M B, Anisimov S I and Fortov V E 2010 *Appl. Phys.* A **101** 1–5
[9] Inogamov N et al. 2011 *Contrib. Plasm. Phys.* **51** 367–374